Machine learning traction force maps for contractile cell monolayers

Changhao Li [a], Luyi Feng [a], Yang Jeong Park [b,c], Jian Yang [d], Ju Li [b], Sulin Zhang [a,d,e,*]

[a] *Department of Engineering Science and Mechanics, Pennsylvania State University, University Park, PA, USA*
[b] *Department of Nuclear Science and Engineering, and Department of Materials Science and Engineering, Massachusetts Institute of Technology, Cambridge, MA 02139, USA*
[c] *Department of Electrical and Computer Engineering, and Institute of New Media and Communications, Seoul National University, Gwanak-gu, Seoul 08826, Republic of Korea*
[d] *Department of Biomedical Engineering, Pennsylvania State University, University Park, PA, USA*
[e] *Department of Material Science and Engineering, Pennsylvania State University, University Park, PA, USA*

ABSTRACT

Machine learning offers immense potential as a transformative tool capable of reshaping optical microscopy and quantitative modeling in cell biology. Here we exemplify this potential through the development of a generative adversarial network (GAN) designed to comprehend and predict cell traction force maps. Empowered by a hybrid dataset from traction force microscopy (TFM) and phase-field modeling (PFM), the GAN learns the intricacies of the traction force maps of contractile cells in complex chemomechanical environments, with the sole input being the phase-contrast images of the cells. The trained GAN accurately predicts collective durotaxis by leveraging the learned asymmetric traction force maps, while also unveiling the concealed correlation between substrate stiffness and cell contractility arising from mechanotransduction. Remarkably, despite its foundation in epithelial cell data, our image-learning algorithm can be extended to other contractile cell types by adjusting a single scaling factor. Our approach underscores the potential of synergizing force microscopies and biophysical models with image-based learning, thus catalyzing data-driven scientific revelations in cell mechanobiology.

1. Introduction

The remarkable ability of cells to perceive, respond, and adapt to mechanical forces constitutes the fundamental aspect of cellular mechanobiology [1–4]. While much has been understood about the intricate interplay between mechanical force transmission and biochemical signaling in cell-cell and cell-extracellular matrix interactions, directing long-range multicellular morphogenesis [5–7], wound healing [8–10], and cancer metastasis [11,12], an in-depth and quantitative understanding of cellular mechanobiology has remained obscure due to the lack of reliable, high-throughput tools for quantifying cellular forces [13–15]. Traction force microscopy (TFM) has been instrumental in measuring the pulling force exerted by focal adhesion points [16–18]. The resultant traction force map lays down the foundation for monolayer stress microscopy (MSM) [19,20] and intercellular tension microscopy (ITM) [21,22,23]. However, TFM involves imaging the traction-induced displacement field of soft substrates inferred by the embedded fluorescent beads and calculating the traction force maps based on the measured displacement fields and mechanical properties of

the substrate. Owing to the complex experimental process, the utility of TFM is constrained by its low throughput [14,24] and diminishing resolution when the stiffness of the extracellular matrix (ECM) exceeds 50 kPa [12,21,25]. These limitations have significantly impeded the advancement of our insights into cellular mechanobiology.

Machine learning (ML) methodologies have ushered in a new era of pattern recognition and image synthesis, achieving unparalleled precision and efficiency [26]. In materials science, substantial strides have been taken in extracting tangible insights from microscopy-driven image learning across various multiple length scales. In contrast, less progress has been made in cell mechanics, perhaps due to the intrinsic complexity of dynamic changes in cell shapes and the cellular forces they generate. ML approaches have recently been developed to deduce traction force maps from the deformation field of cell-seeding substrates [27,28]. Although these methods marked successes to a certain extent, they still rely on imaging the traction-induced displacement field of the substrates, i.e., the wrinkled morphology [27] or displacements inferred by fluorescent beads [28], which represents the most challenging step in classical TFM. Thus, these ML approaches retain inefficiencies and low

---

* Corresponding author at: Department of Engineering Science and Mechanics, Pennsylvania State University, University Park, PA, USA.
   E-mail address: suz10@psu.edu (S. Zhang).

throughput of the classical TFM.

Here, we have developed an ML strategy utilizing a generative adversarial network (GAN) [29] to learn and predict traction force maps of cell monolayers adhering on a flat surface. Our approach diverges from classical TFM and deformation-field-based machine-learning approaches, as it eliminates the need for imaging substrate displacement fields. Instead, our ML approach relies solely on cell contours, substrate stiffness, and cell type as the inputs, markedly increasing its operational efficiency. The GAN model interprets traction force maps as an image-to-image translation task, where its interconnected generative and discriminative neural networks are cooperatively refined through cross-training to reach a converged solution. To address the scarcity of experimental TFM essential for training and validating our neural networks, we resort to a recently established high-throughput biophysical model that produces numerical datasets [21]. Upon training with the hybrid experimental and numerical datasets, our neural network demonstrates its versatility by accomplishing a spectrum of tasks. By integrating TFM, biophysical modeling, and advanced image learning techniques, our method emphasizes the potential of machine learning to unveil complex biomechanical insights from image-derived data in cell mechanobiology.

2. Materials and methods

2.1. Design of computational experiments

To complement the TFM measurements, we construct a database of cell profiles and corresponding traction forces using continuum simulations (Supplementary Information). To generate a sufficiently extensive dataset that covers the latent space of 2D cell profiles, we developed an algorithm to effectively control the regularity and the curvature of randomly generated cell geometries. The algorithm uses a simple descriptor vector $\boldsymbol{d} = (n_s, \overline{R}, r_s, \sigma_s)$, where n_s denotes the number of boundary waves, $\overline{R}$ the effective radius of the cell, r_s the fluctuation for the radius of curvature, and σ_s the Gaussian smoothing parameter. By defining a suitable range and discretized interval for the parameter space embedded in the four-dimensional vector $\boldsymbol{d}$, we generated a cell profile dataset with 8000 samples, which is utilized as the geometry for the continuum model. We developed Python scripts to automate the above algorithm for high-throughput simulations. Further information is available in the Supplementary Information.

2.2. Biophysical model of cell traction forces

The working principle of the classical TFM is to derive traction force maps from the displacement field inferred by fluorescent beads embedded in a soft, deformable substrate. Since cell traction forces displace the beads, detaching cells from the substrate surface eliminates the traction forces, allowing the beads to return to their original, undeformed positions due to the elastic recovery. Solving an inverse elasticity problem relates the measured displacement field to the traction force map. Both cell traction forces sustained at focal adhesion points and viscous forces due to cell migration contribute to the deformation field of the substrate. However, the nonspecific viscous forces are comparably small (Supplementary Information) due to low motility of the migrating cells [30], as validated by the vanishing traction force in regions without focal adhesion points [31]. We further assume that the deformation of the substrate at any instant is small such that linear elasticity applies. It has been suggested that such small deformation is indicative of the cells' instantaneous configuration and the cell shape carries the information about the generated forces [32,33]. The geometry-inferred forces are referred to as "configurational forces", which are central to our continuum model [21] and previous models [34–36]. Our continuum model capitalizes on this concept, i.e., cell shape dictates cell-substrate adhesion forces, to delineate the chemomechanical equilibria of a cell monolayer adhering to a soft substrate. Indeed, these equilibrium conditions yield focal adhesion distributions and traction forces based on the cell substrate stiffness and cell shapes (See Supplementary Information), which agree very well with TFM.

We derived the weak form of governing equations (Supplementary Information) and implemented the corresponding high-throughput simulations by COMSOL Multiphysics package. The input cell geometries are discretized by quadradic triangular elements with appropriate element size balancing the computational cost and simulation accuracy. The Newton-Raphson algorithm is applied to solve the boundary value problem. The output data from COMSOL Multiphysics are postprocessed by Python scripts to fit the format requirements of machine learning libraries.

2.3. Traction force microscopy

We seeded HCT-8 cells onto a soft substrate made of PAA hydrogel at a density of 2000 cells/cm^2. The stiffness of the substrate was controlled by adjusting the concentrations of acrylamide and bis-acrylamide. Prior to cell seeding, we coated the top surface of the substrate with fibronectin. To track the displacements induced by cell traction, we embedded fluorescent beads within a single subplane of the substrate. The seeded HCT-8 cells were then cultured for 24–72 hours until the cell monolayer had sufficiently adhered, spread, and grown into multicellular colonies of varying sizes. A laser-scanning confocal fluorescence microscope (Olympus FV10i, Japan) was utilized to measure the positions of the fluorescent beads with cells adhered to the substrate and detached from the surface, giving rise to the displacement field. An inverse elasticity problem was solved to obtain the cell traction forces.

2.4. Architecture of neural networks

We designed the generator as an adapted U-Net [37], which is an encoder-decoder architecture with a symmetric input and output format. The basic building blocks encoder and decoder of the generator consist of several convolution/max pooling operators and a nonlinear ReLU activation function. The discriminator shares a similar structure to the encoder of the generator. The GAN was implemented based on PyTorch [38], a Python-based deep learning library. After grid-search optimizing [39], we set the training parameter as follows: 200 epochs to stop training, 500 for mini-batch [40] size, ADAM optimizer [41] with the learning rate $\epsilon = 0.0002$, hyperparameters $\beta_1 = 0.6$ and $\beta_2 = 0.95$. The entire training process was deployed on Google Colab.

3. Results and discussion

3.1. Generating hybrid datasets from TFM and phase-field modeling

When seeded on a substrate, migrating cells develop focal adhesion points that pull and deform the substrate. The deformation depends on the pulling force of the cells as well as the mechanical properties of the substrate, i.e., its Young's modulus and Poisson's ratio [12]. For two-dimensional (2D) TFM that measures the tangential pulling force, i. e., traction on flat substrates [16,17], fluorescent beads are embedded into a soft substrate (e.g., hydrogels) to track the traction-induced displacement through an optical microscope, [16,42] in reference to the traction-free condition in which cells are detached off from the substrate. The measured displacement field along with the boundary conditions furnishes an inverse elasticity problem for traction force calculation [12,25]. Using the TFM-reconstructed traction force distribution as a force boundary condition, the stress in the cell body, modeled as a thin monolayer, [20,21,43] can be further determined by monolayer stress microscopy (MSM). The traction force profile indicates focal adhesion distribution [17,44], while the direction of the first principal stress of the cell monolayer infers stress-fiber orientations [20,

45]. For migrating cells, TFM can be applied at different time points, thereby obtaining time-varying traction force maps [46,47].

Training an ML model on high dimensional spaces entails a large dataset for converged model performance. For each cell type, we have no more than 100 experimental traction force maps available up to date, with epithelial cells being the most characterized cell type (Fig. S1). Preparing a large database ($10^3 \sim 10^4$ traction force maps) through experimental TFM is undoubtedly very costly, owing to its low-throughput characteristic. To meet this challenge, we here generated training data by invoking our previously developed continuum model [21]. The continuum model assumes that the traction force distribution of a cell monolayer is determined by its current configuration [34], and imposes the chemomechanical balance laws on the cell-substrate system (Supplementary Information). The continuum model simultaneously yields focal adhesion distributions, monolayer stress distributions, and traction force maps. The predicted traction force maps and monolayer stress distributions (Fig. S2) agree very well with TFM and MSM measurements, respectively [21].

Based on the continuum model, we built a high-throughput simulation workflow to obtain traction force maps with randomly generated cell profiles (Methods, Supplementary Information). The numerical results constitute the main part of the dataset, in addition to the experimental traction force maps from our own group and others. To complement the dataset, we also performed the standard data augmentation algorithm (Supplementary Information) on the limited experimental data. The final dataset includes ~8000 numerical simulations and ~600 experimental TFM measurements. Considering the predominance of the simulation data in the training dataset, we explored the impact of the experimental data by training the same GAN exclusively on a comparably sized dataset derived solely from simulation data. We evaluated the prediction accuracy by comparing it to both simulated and experimental ground truths. The results revealed an increase in the error for experimental data, while the error for the simulated data remained nearly unchanged (Fig. S6). This comparative study underscores the sensitivity of the GAN to data variety within the training set and suggests its potential scalability to extensive experimental datasets.

3.2. Machine-learning algorithms

Here we regard traction force as a configurational force [34], determined by the (current) cell geometry, substrate stiffness, and cell type, which constitute the training data of our ML model. The input cell boundary $r(\theta)$ can be regularized as a $n \times n$ binary geometric indicator tensor $\boldsymbol{\Omega}$ where the element values take 1 inside the cell boundary or 0 otherwise, and n varies for different resolutions. The size of the cell colony, represented by its average radius $\bar{R}$, is given by $\bar{R} = \sqrt{S_{\text{cell}}/\pi}$, where S_{cell} is the area occupied by the cell monolayer. Correspondingly, the traction force vector field $\boldsymbol{T}(\boldsymbol{x})$ can be discretized as a $n \times n \times 2$ tensor, where the two channels in the third dimension represent the traction forces along the in-plane orthogonal directions (x and y directions). Other scalar-valued parameters, such as substrate stiffness, cell radius, and cell contractility, are combined into the aggregated property tensor $\boldsymbol{C}$.

Combining experimental measurements and continuum mechanics modeling, we sample the input space of $\boldsymbol{\Omega}$ and $\boldsymbol{C}$. In experiments, $\boldsymbol{T}$ is directly measured by TFM. In modeling, we use high-throughput simulations to obtain the traction force field $\boldsymbol{T}$ (Fig. 1A, Supplementary Information). Based on the hybrid database, we propose two ML tasks: I) forward problem: given cell geometry $\boldsymbol{\Omega}$ and the parameters $\boldsymbol{C}$, predict the traction force map $\boldsymbol{T} = f(\boldsymbol{\Omega}, \boldsymbol{C})$; II) inverse problem: given $\boldsymbol{T}$ and $\boldsymbol{\Omega}$, predict a set of parameters $\boldsymbol{C} = \hat{f}(\boldsymbol{\Omega}, \boldsymbol{T})$, some of which are hidden relationships that are inaccessible to experiments and underlie cellular mechanotransduction.

For task I, we recast the prediction of traction force maps from given cell geometry as the image-image translation problem [48] in computer
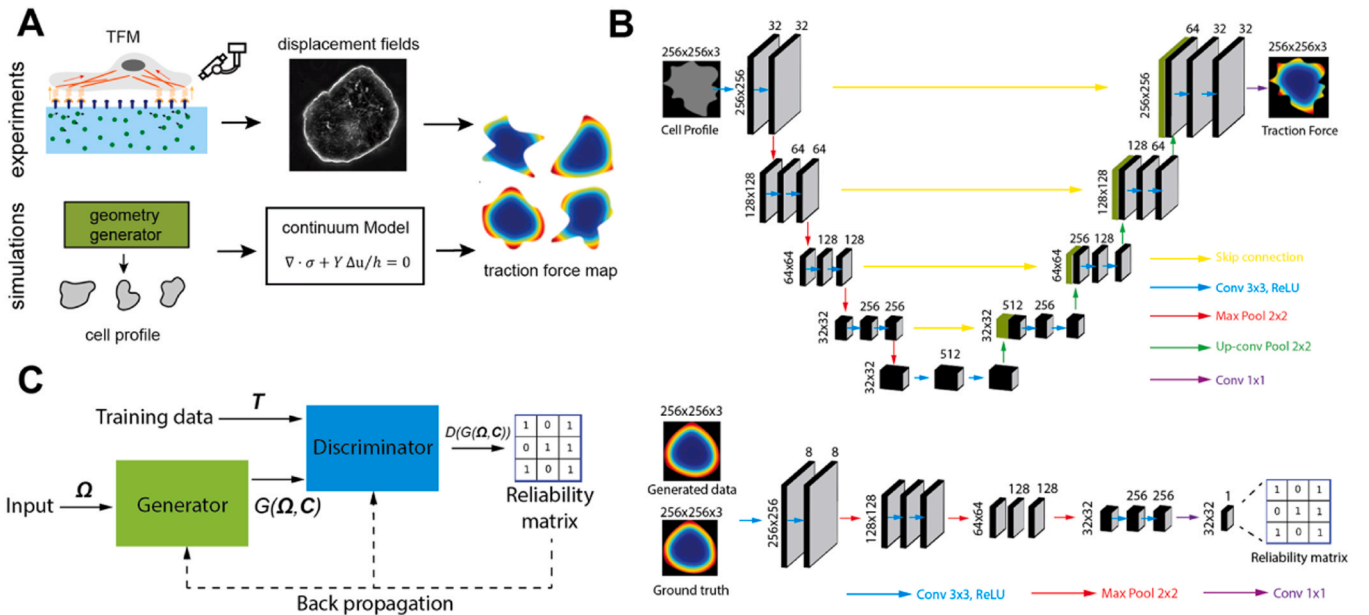

Fig. 1. Schematic illustration of the data collection processes and the generative adversarial network (GAN). A. The hybrid data generation processes from TFM experiments and high-throughput simulations. **B.** Top: The architecture of the generator. 3D image tensors are visualized as black cuboids labeled with their size, and neural network operators are represented as arrows with different colors. Yellow arrow: skip connection operator which skips middle network blocks and directly concatenates the input tensor to its output. Blue arrow: 3×3 convolution operator followed by ReLU activation function, which shrinks the first two dimensions and expands the third dimension of the input tensor. Red arrow: max pooling operator which is similar to the convolution operator but takes the local maximum value. Green arrow: up-convolution operator, which is the inverse operator of convolution. Purple arrow: 1×1 convolution operator, which only shrinks the third dimension and leaves the first two dimensions unchanged. Bottom: The architecture of the discriminator. The information flow and data structure are displayed in a similar way as in the generator. **C.** The training workflow of the GAN. Solid arrows denote forward propagation and dashed arrows denote backpropagation.

vision technology. Inspired by the recent progress in image generation [49] and style transfer [50], we designed a generative adversarial network (GAN) to extract the underlying distribution patterns of traction force. A GAN consists of a generative (generator) and a discriminative (discriminator) neural network, where the generator and the discriminator compete and evolve together to reach a final converged image. Upon training, the generator gains an increasing ability to generate artificial data that can effectively fool the discriminator. When the discriminator can no longer effectively distinguish the difference between the ground-truth data and artificial data generated by the generator, the cross-training converges. As shown in Fig. 1B-C, our generator is adapted from U-Net [37], a classical convolutional neural network (CNN) widely applied in biomedical image segmentation tasks, and our discriminator is composed of a CNN linked to a fully connected neural network. The loss function $L(D, G)$ of the GAN can be formulated by the cross entropy formulation,

$$L(D, G) = \mathbb{E}_{T \sim p(T)}[\log(D(T))] + \mathbb{E}_{\Omega, C \sim p(\Omega, C)}[\log(1 - D(G(\Omega, C)))], \quad (1)$$

where D and G represent the discriminator and generator, respectively, $p(T)$ and $p(\Omega, C)$ are distributions of the ground truth and the input data, respectively, and $\mathbb{E}$ denotes the pixelwise average over the training set. Fig. 1C shows the workflow and dataflow of the proposed GAN, where the gradients of $L(D, G)$ backpropagate to the discriminator D and the generator G, enabling their simultaneous training process: $\max_D \min_G L(D, G)$. The discriminator outputs a binary reliability matrix indicating the extent of "validity" of local segments of the input images (Fig. 1B), while the generator G predicts the traction force map T from the given cell geometry Ω and the property tensor C.

3.3. Learning the traction force maps for epithelial cell colonies

As shown in Fig. 1, we train the GAN on the hybrid database (Methods and Supplementary Information), which includes simulated and experimentally measured traction force maps for different cell colony sizes and substrate stiffnesses. Our training data are solely based on epithelial cells, as this cell type has the most available datasets of experimental traction force maps. The traction force map predicted by GAN shows great consistency with both simulation and TFM results for different colony sizes (Fig. 2A) and substrate stiffnesses (Fig. 2B). The overall profile of predicted traction force magnitude follows a similar trend of exponential decay from the cell periphery to its center and accumulates in the boundary regions with higher local convex curvature (Fig. 2A-B, Fig. S3). The above two features of traction force distribution can also be clearly observed from the intermediate feature maps (Fig. S4) from the trained generator. Based on the error heatmaps (Fig. 2C-D, Fig. S5), we found that the ML model successfully captured the distinctive features of the traction force maps, including the localized traction force at the edges of cell monolayer and negligible traction within the interior region. Despite the overall trend of our ML predicted traction force distribution being consistent with the experimental data, we have noted a pronounced relative error in the central region of the cell monolayers. The primary factor contributing to this relative error is the inherently low traction force at the central region of the monolayers. The discrepancies between our ML model predictions and experimental data are largely attributed to the divergence of our simulation-dominated training dataset from experimental data. In our continuum model, which constitutes the bulk of the training set, we assume perfect cell-cell adhesion and omit the viscous forces associated with cell mobility. Both factors contribute to the variations of traction forces [6, 51], albeit minor.

We then define the average pixelwise error by $\epsilon_T = \frac{1}{n^2 N} \Sigma_N \left(\left| \left(T_{ijk}^p - T_{ijk}^t \right) \right| / \left| T_{ijk}^t \right| \right)$, where T_{ijk} denotes the components of the ML-predicted (T_{ijk}^p) or the ground-truth (T_{ijk}^t) traction force tensor, and N is the size of the training set. ϵ_T was measured separately on the test
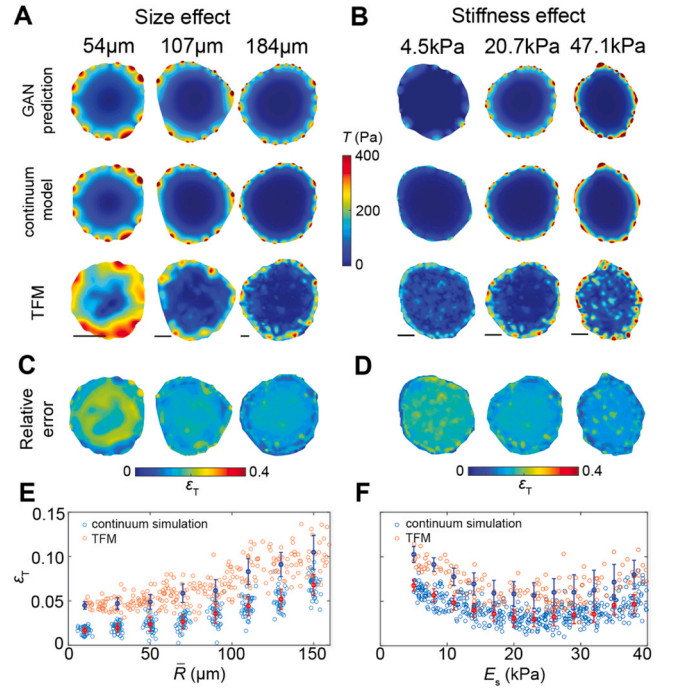

Fig. 2. ML prediction on the dependences of traction force maps on monolayer size and substrate stiffness. **A.** Effect of cell colony size. The traction force maps for cell colonies with different average radii (54 μm, 107 μm, and 184 μm) are measured by TFM (bottom row), simulated (middle row) by the continuum model, and predicted by the ML model (top row). Scale bar: 20 μm. **B.** Effect of substrate stiffness. Colormaps are measured, simulated, and ML predicted traction force maps of cell colonies with different substrate stiffness (4.5kPa, 20.7kPa, and 47.1kPa), respectively. Scale bar: 20 μm. **C-D.** Spatial heatmaps of the relative error ϵ_T between GAN prediction and experimental TFM for size effect (**C**) and substrate stiffness effect (**D**). **E.** Spatial averaged relative prediction error ϵ_T of our ML model for different average cell colony sizes $\bar{R}$ in comparison to TFM and continuum modeling. **F.** Spatial averaged relative prediction error ϵ_T for various substrate stiffnesses. Blue (red) error bar denotes the average and standard deviation of ϵ_T from experiments (simulations).

datasets from the continuum simulation and TFM experiments. We found that for all cases $\epsilon_T < 15\%$ and monotonically increases with the colony size $\bar{R}$ (Fig. 2E), but relatively stable with substrate stiffness E_s (Fig. 2F). Indeed, given a fixed size n of geometry indicator Ω, a larger $\bar{R}$ corresponds to downsampling and hence decreases resolution. As expected, the GAN achieves better performance on the simulation test set, which constitutes the main part of the training data.

3.4. Learning the asymmetric traction force distribution that implicates durotaxis

In durotaxis, migrating cells sense and follow environmental stiffness gradient [52,53], exhibiting an asymmetrically localized traction force distribution at the leading and trailing edges that signifies cell migration direction [52,54]. The asymmetric traction force distribution can be attributed to the maturation of focal adhesion points from which lamellipodia extend forward for cell crawling [55,56]. Here we explore if our ML model can predict the traction force localization $T_{pred}(x) = f(E_s(x), \Omega)$ with given substrate gradient $\nabla E_s(x)$ and cell geometry Ω (Fig. 3A). We sample the input space of $E_s(x)$ by 5000 additional simulations and train the GAN on the Supporting Information set. Fig. 3B shows that our ML model captures the asymmetric traction force distribution of the cell monolayer on a substrate with a stiffness gradient, where we specifically chose several relatively symmetrical colony profiles (as detailed in Supplementary Information) to minimize the
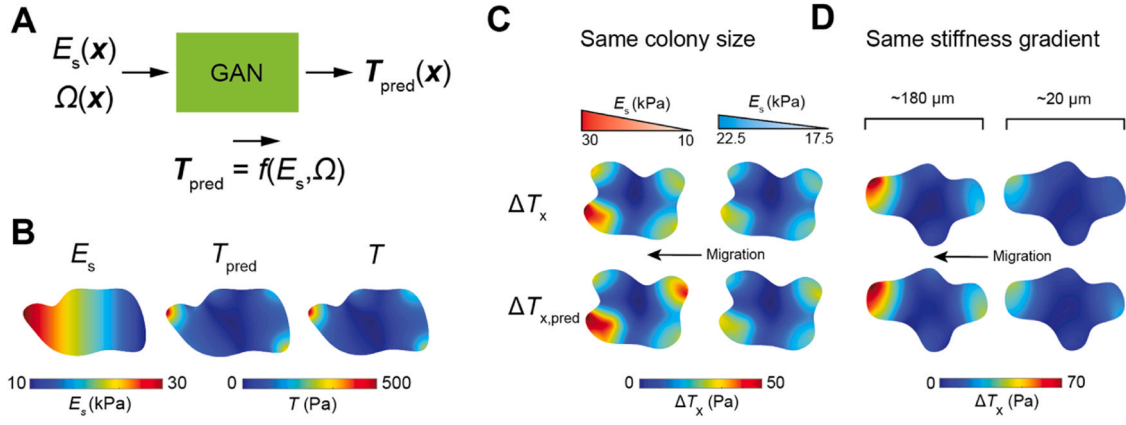
Fig. 3. The extended ML model predicts collective durotaxis. **A.** Schematic illustration of forward prediction of traction force maps. **B.** An ML predicted traction force map $T_{pred}(x)$ from forward prediction with spatially varying substrate stiffness, in good comparison to the continuum simulations. **C-D.** Machine learning predicting collective durotaxis effects. The predicted traction force difference $\Delta T_x(x)$ shows clear localization at the stiff side. The traction force localization becomes more pronounced with increasing stiffness gradient (**C**) and cell colony size (**D**).

influence of cell profiles on the traction force maps. Specifically, traction force localization occurs more predominantly on the stiff side of the substrate, indicating soft-to-rigid cell migration direction, i.e., durotaxis, consistent with the reported experimental observations [52,54, 57].

It was previously revealed that collective durotaxis arises from long-range transmission of intercellular forces, where a multicellular colony can sense weak stiffness gradient of the substrate but isolated individual cells cannot [52,57]. To see whether our ML model can predict collective durotaxis, here we vary substrate stiffness gradient (Fig. 3C) and colony size (Fig. 3D) and quantify the traction force difference $\Delta T = T_G - T_0$, where T_G and T_0 are the predicted traction force maps by our ML model for the same cell colony on the substrate with stiffness gradient and uniform substrate with the same average stiffness, respectively. In Fig. 3C-D, we visualize the horizontal component of ΔT, ΔT_x, the same direction as the stiffness gradient. Our ML model predicts pronounced localization of traction forces at the stiff side with increasing substrate stiffness gradient and cell colony size. As lamellipodia extend from the localization sites of traction force, our prediction indicates collective

durotaxis, consistent with previously reported results [52].

3.5. Extracting the relation between substrate stiffness and cell contractility

Cells sense and adapt to their mechanical environments by operating their contractile machinery at different levels through mechanotransduction [6,58,59]. Thus, cell contractility and substrate stiffness are intimately correlated [60,61], though it remains a challenge to quantify such a relationship experimentally. Here we recast our ML task to (II), inversely predicting hidden correlations using traction force map T: $C = \hat{f}(\Omega, T)$. In the inverse prediction, traction force maps are taken as known data, but $E_s(x)$ and the cell contractility σ_A are variables to be learned (Fig. 4A). Similarly, by resorting to the continuum simulations, we sample the input spaces of T, Ω and the corresponding output σ_A and $E_s(x)$, and train a U-Net on this dataset (Supplementary Information). Fig. 4B shows full-field stiffness prediction for circular and linear patterning modes of substrate stiffness, and the GAN prediction shows good accuracy on a wide range of colony shapes and substrate stiffness
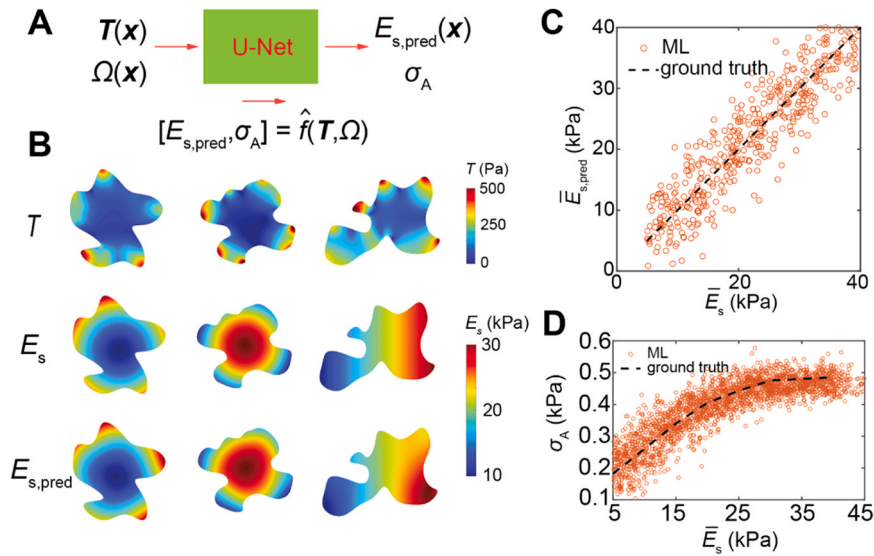

Fig. 4. ML prediction of the hidden properties of the cell-substrate system. **A.** Schematic illustration of inverse prediction of cell and substrate properties. **B.** Full-field stiffness prediction results for circular and linear patterning modes of substrate stiffness. **C.** ML regression of spatially averaged stiffness $\bar{E}_s$. The data range for ground truth is computationally generated from 5kPa to 40kPa. **D.** The $\sigma_A - \bar{E}_s$ relation captured by the ML model (hollow scatters), compared with the ground truth generated by simulation (dashed line).

patterns (Supplementary Information). Our machine learning prediction for $E_s(x)$ shows qualitative consistency for the whole range of substrate stiffnesses, and successfully captures the spatial variations of substrate stiffness. Fig. 4C displays the comparison between the ground truth of the substrate modulus $\bar{E}_s$ used in continuum simulations and the predicted $\bar{E}_{s,pred}$. Furthermore, we find that the U-Net can learn the underlying nonlinear function between active stress σ_A and the substrate stiffness E_s (Fig. 4D). This inverse procedure provides a new route to estimate spatially varying properties of the cell-substrate system.

3.6. Extrapolating the image-learning approach to other cell types

Contractile cells of different types share similar mechano-biochemical feedback loops in traction force generation [65,66], despite cell-type dependent contractility σ_A is different in response to the local mechanical environments such as substrate stiffness. From a biophysical perspective, cells are powered by actomyosin motors, which generate cell contractility [67]. This contractile force is then transmitted not only to the extracellular matrix, generating traction, but also to the intercellular adherens junctions, generating intercellular tension [6]. Cell contractility is closely linked to the self-assembly of the actin cytoskeleton, thereby influencing the cell modulus. Cell contractility is also correlated to the level of cell spreading: the higher cell contractility, the more spreading the cell [68]. Cells can sense and adapt to substrate stiffness by varying their level of contractility through mechano-transduction [69]. Thus, these cellular properties are inherently related to cell contractility. Surface tension may appear to be independent of cell contractility. However, from our parameter-sensitivity studies (Fig. S7), surface tension does not significantly alter traction force maps.

From these analyses, cell contractility emerges as the crucial parameter for characterizing force distribution with given cell profiles. Thus, we rationalize that traction force maps for all the types of contractile cells have similar spatial patterns, but scale with cell-type dependent contractility σ_A. This provides a convenient route to further extend our ML model to other contractile cell types. Without any retraining, we directly scale the trained GAN to four different cell types (fibroblast [62], Hela [63], MDCK [23], and Osteosarcoma [64] cell lines) by a constant α and compare the prediction with the reported experimental measurements (Fig. 5A-B). The scaling factor α is defined as the contractility of the specific cell types relative to that of HCT-8 epithelial cells. As expected, the predicted traction force maps of the GAN, which are only trained on HCT-8 epithelial datasets, have reasonably good agreement with the experimental measurements, demonstrating the transferrable learning abilities of our ML model.

4. Conclusions

In summary, the generative adversarial network (GAN), trained using a combination of experimental and numerical datasets, adeptly generates a good estimation of traction force maps from just cell contours as inputs. Given that the continuum model involves the coupling of multi-field partial differential equations (PDEs), our ML framework serves as a surrogate model for these complex PDEs. Beyond its ability to predict substrate-stiffness and colony-size dependent traction force maps, the neural network uncovers the elusive relationship between substrate stiffness and cell contractility, an aspect pivotal to cell mechanobiology but often difficult to measure experimentally. Remarkably, the ML model, without any alternation to its architecture, effectively forecasts asymmetric traction force distribution when cells adhere to a substrate with stiffness gradient, demonstrating its capability to predict collective durotaxis. Additionally, despite being trained exclusively on epithelial cell data, our ML model can be seamlessly extended to other contractile cell types by adjusting a single scaling factor specific to each cell type. Collectively, our work establishes a potent digital TFM (DTFM) approach for comprehensively mapping traction forces of contractile cell monolayers.

Despite accurately replicating the biophysical continuum model and capturing the overall patterns of experimental traction force distributions, our ML model still encounters challenges with accurately pinpointing local force concentrations and their spatial fluctuations. Part of the discrepancy arises from the simplification of the continuum model, which does not account for the complexities such as the variability of cell-cell adhesion [6] and the viscous force [51] associated with cell motility. Additionally, the noise within experimental data intrinsic to TFM complicates the task for ML models to precisely map traction forces. This presents both challenges and opportunities to improve the biophysics model, refine the ML approach, and strengthen their integration for enhanced model interpretability and generalizability.

The proposed DTFM can be extended to biologically richer datasets, such as linking the focal adhesion distribution and actin cytoskeleton organization to the traction force map. Furthermore, the DTFM can be adapted to predict the time-evolving traction forces for migrating cells, a
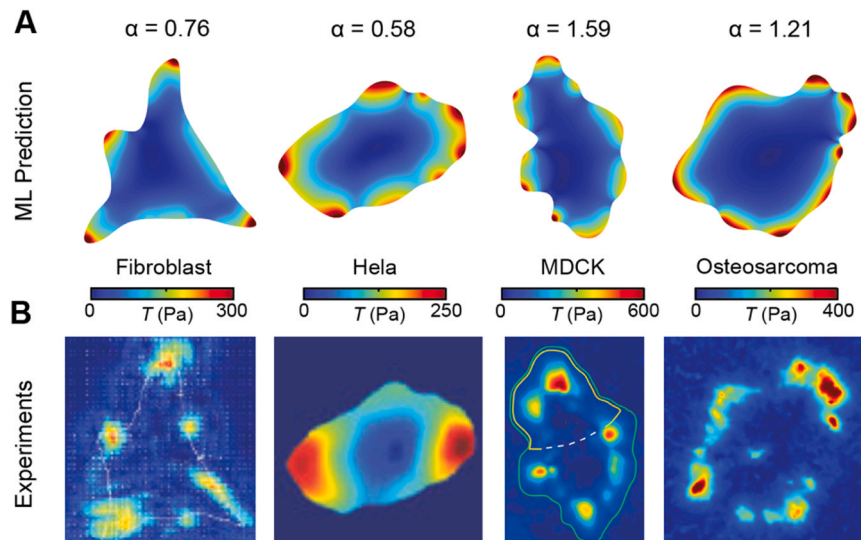

Fig. 5. Extrapolation of the ML model to other contractile cell types. A-B. Representative prediction results (**A**) from the GAN, and the comparison (**B**) between experiments. Here α is a scaling factor that accounts for cell-type dependent contractility. Cell geometries and traction force maps of fibroblast [62], Hela [63], MDCK [23] and Osteoarcoma [64] are extracted from previous studies.

straightforward extension due to the sole requirement of cell contours as input. Given that traction force distribution forms the foundation for assessing cell monolayer stress and intercellular tension, the established DTFM significantly advances the development of digital MSM and IFM, culminating in a comprehensive toolset for extra-, intra- and inter-cellular force measurements. These digital force microscopy techniques hold immense potential to expedite and refine scientific break-throughs, particularly concerning the pivotal role of mechanical forces in intricate mechanobiochemical processes such as collective cell migration [52,70,71], multicellular morphogenesis [5,72], and cancer metastasis [11,12,56], among others.

CRediT authorship contribution statement

Changhao Li: Data curation, Formal analysis, Investigation, Soft-ware, Writing – original draft, Writing – review & editing. **Luyi Feng:** Data curation, Formal analysis, Software, Writing – original draft, Writing – review & editing. **YangJeong Park:** Formal analysis, Meth-odology, Software. **Jian Yang:** Funding acquisition, Resources, Valida-tion. **Ju Li:** Conceptualization, Formal analysis, Investigation, Software, Writing – review & editing. **Sulin Zhang:** Conceptualization, Formal analysis, Funding acquisition, Investigation, Methodology, Project administration, Resources, Supervision, Validation, Writing – original draft, Writing – review & editing.

Declaration of Competing Interest

The authors declare that they have no known competing financial interests or personal relationships that could have appeared to influence the work reported in this paper.

Data availability

Data will be made available on request.

Acknowledgments

Appendix A. Supporting information

Supplementary data associated with this article can be found in the online version at doi:10.1016/j.eml.2024.102150.

References

[1] V. Vogel, M. Sheetz, Local force and geometry sensing regulate cell functions, Nat. Rev. Mol. Cell Biol. 7 (2006) 265–275.

[2] J. Fu, et al., Mechanical regulation of cell function with geometrically modulated elastomeric substrates, Nat. Methods 7 (2010) 733–736.

[3] M. Ghibaudo, et al., Traction forces and rigidity sensing regulate cell functions, Soft Matter 4 (2008) 1836–1843.

[4] X. Trepat, et al., Physical forces during collective cell migration, Nat. Phys. 5 (2009) 426–430.

[5] T. Lecuit, P.F. Lenne, Cell surface mechanics and the control of cell shape, tissue patterns and morphogenesis, Nat. Rev. Mol. Cell Biol. 8 (2007) 633–644.

[6] B. Ladoux, R.M. Mège, Mechanobiology of collective cell behaviours, Nat. Rev. Mol. Cell Biol. 18 (2017) 743–757.

[7] S.R.K. Vedula, et al., Epithelial bridges maintain tissue integrity during collective cell migration, Nat. Mater. 13 (2014) 87–96.

[8] M. Tamada, T.D. Perez, W.J. Nelson, M.P. Sheetz, Two distinct modes of myosin assembly and dynamics during epithelial wound closure, J. Cell Biol. 176 (2007) 27–33.

[9] M.S. Sakar, J. Eyckmans, R. Pieters, D. Eberli, B.J. Nelson, C.S. Chen, Cellular forces and matrix assembly coordinate fibrous tissue repair, Nat. Commun. 7 (2016) 11036.

[10] A. Ravasio, et al., Gap geometry dictates epithelial closure efficiency, Nat. Commun. 6 (2015) 7683.

[11] J.M. Tse, et al., Mechanical compression drives cancer cells toward invasive phenotype, Proc. Natl. Acad. Sci. USA 109 (2012) 911–916.

[12] Y. Zhang, et al., A traction force threshold signifies metastatic phenotypic change in multicellular epithelia, Soft Matter 15 (2019) 7203–7210.

[13] W.J. Polacheck, C.S. Chen, Measuring cell-generated forces: a guide to the available tools, Nat. Methods 13 (2016) 415–423.

[14] T. Ando, et al., The 2018 correlative microscopy techniques roadmap, J. Phys. D. Appl. Phys. 51 (2018) 443001.

[15] P. Roca-Cusachs, V. Conte, X. Trepat, Quantifying forces in cell biology, Nat. Cell Biol. 19 (2017) 742–751.

[16] R.W. Style, et al., Traction force microscopy in physics and biology, Soft Matter 10 (2014) 4047–4055.

[17] B. Sabass, M.L. Gardel, C.M. Waterman, U.S. Schwarz, High resolution traction force microscopy based on experimental and computational advances, Biophys. J. 94 (2008) 207–220.

[18] M. Dembo, Y.L. Wang, Stresses at the cell-to-substrate interface during locomotion of fibroblasts, Biophys. J. 76 (1999) 2307–2316.

[19] D.T. Tambe, et al., Monolayer stress microscopy: limitations, artifacts, and accuracy of recovered intercellular stresses, PloS One 8 (2013) e55172.

[20] D.T. Tambe, et al., Collective cell guidance by cooperative intercellular forces, Nat. Mater. 10 (2011) 469–475.

[21] T. Zhao, et al., Active cell-matrix coupling regulates cellular force landscapes of cohesive epithelial monolayers, Npj Comput. Mater. 4 (2018) 10.

[22] M.R. Ng, A. Besser, J.S. Brugge, G. Danuser, Mapping the dynamics of force transduction at cell-cell junctions of epithelial clusters, Elife 3 (2014) e03282.

[23] V. Maruthamuthu, B. Sabass, U.S. Schwarz, M.L. Gardel, Cell-ECM traction force modulates endogenous tension at cell–cell contacts. Proc. Natl. Acad. Sci. 108 (2011) 4708–4713.

[24] J.W. Blumberg, U.S. Schwarz, Comparison of direct and inverse methods for 2.5D traction force microscopy, Plos One 17 (2022) e0262773.

[25] S.V. Plotnikov, B. Sabass, U.S. Schwarz, C.M. Waterman. High-resolution traction force microscopy, Methods in Cell Biology, Academic Press, 2014, pp. 367–394.

[26] K.T. Butler, D.W. Davies, H. Cartwright, O. Isayev, A. Walsh, Machine learning for molecular and materials science, Nature 559 (2018) 547–555.

[27] H. Li, et al., Wrinkle force microscopy: a machine learning based approach to predict cell mechanics from images, Commun. Biol. 5 (2022) 361.

[28] Y.L. Wang, Y.C. Lin, Traction force microscopy by deep learning, Biophys. J. 120 (2021) 3079–3090.

[29] I. Goodfellow, et al., Generative adversarial networks, Commun. ACM 63 (2020) 139–144.

[30] X. Tang, et al., Mechanical force affects expression of an in vitro metastasis-like phenotype in HCT-8 cells, Biophys. J. 99 (2010) 2460–2469.

[31] Q. Wei, et al., Mechanotargeting: mechanics-dependent cellular uptake of nanoparticles, Adv. Mater. 30 (2018) 1707464.

[32] N. Gov, Guided by curvature: shaping cells by coupling curved membrane proteins and cytoskeletal forces, Philos. Trans. R. Soc. B: Biol. Sci. 373 (2018) 20170115.

[33] A.D. Rape, W.H. Guo, Y.L. Wang, The regulation of traction force in relation to cell shape and focal adhesions, Biomaterials 32 (2011) 2043–2051.

[34] I.B. Bischofs, S.S. Schmidt, U.S. Schwarz, Effect of adhesion geometry and rigidity on cellular force distributions, Phys. Rev. Lett. 103 (2009) 048101.

[35] A.F. Mertz, et al., Scaling of traction forces with the size of cohesive cell colonies, Phys. Rev. Lett. 108 (2012) 198101.

[36] S. Safran, N. Gov, A. Nicolas, U.S. Schwarz, T. Tlusty, Physics of cell elasticity, shape and adhesion, Phys. A: Stat. Mech. its Appl. 352 (2005) 171–201.

[37] O. Ronneberger, P. Fischer, T. Brox. U-net: Convolutional networks for biomedical image segmentation. In: Medical Image Computing and Computer-Assisted Intervention–MICCAI 2015: 18th International Conference, Munich, Germany, October 5-9, 2015, Proceedings, Part III 18, Springer (2015) 234-341.

[38] A. Paszke, et al., Pytorch: An imperative style, high-performance deep learning library, Adv. Neural Inf. Process. Syst. 32 (2019).

[39] M. Feurer, F. Hutter, Hyperparameter optimization, Autom. Mach. Learn.: Methods, Syst., Chall. (2019) 3–33.

[40] G. Hinton, N. Srivastava, K. Swersky, Neural networks for machine learning lecture 6a overview of mini-batch gradient descent, Cited on 14 (2012) 2.

[41] D.P. Kingma, J. Ba, ADAM: A method for stochastic optimization, arXiv (2014) 14126980.

[42] M. Dembo, T. Oliver, A. Ishihara, K. Jacobson, Imaging the traction stresses exerted by locomoting cells with the elastic substratum method, Biophys. J. 70 (1996) 2008–2022.

[43] S.S. Hur, et al., Roles of cell confluency and fluid shear in 3-dimensional intracellular forces in endothelial cells, Proc. Natl. Acad. Sci. 109 (2012) 11110–11115.

[44] M.A. Wozniak, K. Modzelewska, L. Kwong, P.J. Keely, Focal adhesion regulation of cell behavior, Biochim. Et. Biophys. Acta (BBA)-Mol. Cell Res. 1692 (2004) 103–119.

[45] H. Yuan, B. Marzban, K.K. Parker, Myofibrils in cardiomyocytes tend to assemble along the maximal principle stress directions, J. Biomech. Eng. - Trans. Asme 139 (2017) 121010.

[46] S. Munevar, Y.L. Wang, M. Dembo, Traction force microscopy of migrating normal and H-ras transformed 3T3 fibroblasts, Biophys. J. 80 (2001) 1744–1757.

[47] H. Delanoe-Ayari, J.P. Rieu, M. Sano, 4D traction force microscopy reveals asymmetric cortical forces in migrating dictyostelium cells, Phys. Rev. Lett. 105 (2010) 248103.

[48] M.Y. Liu, T. Breuel, J. Kautz, Unsupervised image-to-image translation networks, Adv. Neural Inf. Process. Syst. 30 (2017).

[49] J. Bao, D. Chen, F. Wen, H. Li, G. Hua, CVAE-GAN: Fine-grained image generation through asymmetric training, in: Proceedings of the IEEE International Conference On Computer Vision (2017) 2745–2754.

[50] A. Almahairi, S. Rajeshwar, A. Sordoni, P. Bachman, A. Courville, Augmented cyclegan: Learning many-to-many mappings from unpaired data. In: *International conference on machine learning* , PMLR (2018) 195–204.

[51] E.N. Schaumann, M.F. Staddon, M.L. Gardel, S. Banerjee, Force localization modes in dynamic epithelial colonies, Mol. Biol. Cell 29 (2018) 2835–2847.

[52] R. Sunyer, et al., Collective cell durotaxis emerges from long-range intercellular force transmission, Science 353 (2016) 1157–1161.

[53] A. Shellard, R. Mayor, Collective durotaxis along a self-generated stiffness gradient in vivo, Nature 600 (2021) 690–694.

[54] M.T. Breckenridge, R.A. Desai, M.T. Yang, J.P. Fu, C.S. Chen, Substrates with engineered step changes in rigidity induce traction force polarity and durotaxis, Cell. Mol. Bioeng. 7 (2014) 26–34.

[55] B.J. DuChez, A.D. Doyle, E.K. Dimitriadis, K.M. Yamada, Durotaxis by human cancer cells, Biophys. J. 116 (2019) 670–683.

[56] J.T. Parsons, A.R. Horwitz, M.A. Schwartz, Cell adhesion: integrating cytoskeletal dynamics and cellular tension, Nat. Rev. Mol. Cell Bio 11 (2010) 633–643.

[57] B.C. Isenberg, P.A. DiMilla, M. Walker, S. Kim, J.Y. Wong, Vascular smooth muscle cell durotaxis depends on substrate stiffness gradient strength, Biophys. J. 97 (2009) 1313–1322.

[58] V.B. Shenoy, H. Wang, X. Wang, A chemo-mechanical free-energy-based approach to model durotaxis and extracellular stiffness-dependent contraction and polarization of cells, Interface Focus 6 (2016) 20150067.

[59] B. Ladoux, R.M. Mège, X. Trepat, Front–rear polarization by mechanical cues: from single cells to tissues, Trends Cell Biol. 26 (2016) 420–433.

[60] L.M. Owen, et al., A cytoskeletal clutch mediates cellular force transmission in a soft, three-dimensional extracellular matrix, Mol. Biol. Cell 28 (2017) 1959–1974.

[61] J.R.D. Soine, C.A. Brand, J. Stricker, P.W. Oakes, M.L. Gardel, U.S. Schwarz, Model-based traction force microscopy reveals differential tension in cellular actin bundles, Plos Comput. Biol. 11 (2015) e1004076.

[62] T. Das, T.K. Maiti, S. Chakraborty, Traction force microscopy on-chip: shear deformation of fibroblast cells, Lab a Chip 8 (2008) 1308–1318.

[63] Z. Li, et al., Quantifying the traction force of a single cell by aligned silicon nanowire array, Nano Lett. 9 (2009) 3575–3580.

[64] A. Stubb, et al., Fluctuation-based super-resolution traction force microscopy, Nano Lett. 20 (2020) 2230–2245.

[65] J.H. Wang, J.S. Lin, Cell traction force and measurement methods, Biomech. Model. Mechanobiol. 6 (2007) 361–371.

[66] V.S. Deshpande, R.M. McMeeking, A.G. Evans, A bio-chemo-mechanical model for cell contractility, Proc. Natl. Acad. Sci. 103 (2006) 14015–14020.

[67] M. Murrell, P.W. Oakes, M. Lenz, M.L. Gardel, Forcing cells into shape: the mechanics of actomyosin contractility, Nat. Rev. Mol. Cell Biol. 16 (2015) 486–498.

[68] L. Trichet, et al., Evidence of a large-scale mechanosensing mechanism for cellular adaptation to substrate stiffness, Proc. Natl. Acad. Sci. 109 (2012) 6933–6938.

[69] S. Wong, W.H. Guo, Y.L. Wang, Fibroblasts probe substrate rigidity with filopodia extensions before occupying an area, Proc. Natl. Acad. Sci. 111 (2014) 17176–17181.

[70] P. Friedl, D. Gilmour, Collective cell migration in morphogenesis, regeneration and cancer, Nat. Rev. Mol. Cell Bio 10 (2009) 445–457.

[71] O. du Roure, et al., Force mapping in epithelial cell migration, Proc. Natl. Acad. Sci. USA 102 (2005) 2390–2395.

[72] J. Nijjer, C. Li, Q. Zhang, H. Lu, S. Zhang, J. Yan, Mechanical forces drive a reorientation cascade leading to biofilm self-patterning, Nat. Commun. 12 (2021) 1–9.